

Nodal-line semimetals and their variance

Po-Yao Chang^{1,2,*}

¹*Department of Physics, National Tsing Hua University, Hsinchu 30013, Taiwan*

²*Yukawa Institute for Theoretical Physics, Kyoto University, Kyoto 606-8502, Japan*

(Dated: July 4, 2025)

Topological nodal-line semimetals (NLSMs) are a new family of topological materials characterized by electronic band crossings that form lines in the Brillouin zone. These NLSMs host exotic nodal-line structures and exhibit distinct features such as drumhead surface states and unique electromagnetic responses. This review classifies various NLSM types based on their nodal structures and protecting symmetries, highlighting that these nodal-line structures can form links, knots, and chains. We discuss their characteristic electromagnetic responses, including Landau level spectroscopy, optical conductivity, and permittivity. Furthermore, the strong correlation effects in these NLSMs modify their semimetallic phases and lead to novel quantum phases where magnetism and superconductivity intertwine.

I. INTRODUCTION

The quest for novel quantum states of matter, driven by the intricate interplay of symmetry, topology, and quantum mechanics, is a central theme in modern condensed matter physics. Among the most fascinating discoveries in recent decades is the emergence of topological materials, which host exotic phases characterized by unique electronic structures and protected boundary phenomena. Prominent examples include topological insulators (TIs), featuring insulating bulk states but conductive surface states whose transport properties are remarkably robust against non-magnetic disorder, offering potential pathways towards dissipationless electronics [1–3]. Another key family is Weyl semimetals (WSMs), characterized by bulk band-touching points (Weyl nodes) that act as sources or sinks of Berry curvature, leading to unique electromagnetic phenomena rooted in fundamental chiral anomalies, observable through signatures like the chiral magnetic effect-induced negative magnetoresistance [4]. The profound physics and potential application of these topological properties in areas ranging from low-power electronics to quantum computing have spurred significant theoretical and experimental interest across diverse research fields.

Beyond the point-like nodes of WSMs, a distinct class of topological gapless systems emerged: topological nodal-line semimetals (NLSMs), first proposed theoretically in Ref. [5]. These materials are distinguished by their electronic band structures where conduction and valence bands touch not at isolated points, but along continuous lines or loops within the three-dimensional Brillouin zone (BZ). This distinct nodal structure, protected by symmetries like mirror reflection or time-reversal combined with inversion, imparts unique characteristics. Similar to their topological counterparts, NLSMs possess protected surface states, which often manifest as two-dimensional ‘drumhead’ states spanning the region enclosed by the projection of the bulk nodal lines onto the surface BZ [5–24]. These surface states represent a key experimental fingerprint. Furthermore, NLSMs can exhibit unique magneto-transport phenomena, including distinct quantum os-

cillations and zeroth Landau level physics related to the quasi-relativistic dispersion near the nodal lines, conceptually linked to behaviors observed in layered graphene systems [25, 26]. Crucially, the predicted drumhead surface states, a hallmark of NLSMs, have been experimentally resolved using Angle-Resolved Photoemission Spectroscopy (ARPES) in several candidate materials [8], solidifying their physical realization.

Over the past decade, research on NLSMs has rapidly evolved from theoretical proposals to material discovery and characterization. This progress has been charted in several valuable review articles that have summarized key developments. These include discussions on the theoretical foundations and topological classification schemes [12], the prediction and identification of NLSM material candidates using first-principles calculations [27], explorations of unique quantum transport signatures [28], realizations of nodal-line physics in artificial structures like photonic and phononic crystals [29], and comprehensive overviews connecting experimental confirmations with theoretical predictions [30]. While these reviews provide essential perspectives, the field continues to advance rapidly, particularly regarding the diversity of NLSM types and the interplay with interactions.

This review aims to complement the existing literature by providing a focused discussion of various distinct types of NLSMs based on their nodal structures and protecting symmetries. We will delve into their characteristic electromagnetic responses, which serve as powerful probes of their underlying topological nature and band structure. Furthermore, we place particular emphasis on the influence of electron-electron correlation effects in NLSMs, an increasingly critical area exploring how interactions can modify the semimetallic state, potentially driving transitions to novel correlated or symmetry-broken phases. By concentrating on these interconnected aspects, e.g., classification, electromagnetic response, and correlations, we aim to provide an updated perspective on the rich physics harbored within nodal-line semimetals.

II. NODAL-LINE SEMIMETALS (NLSMS)

We briefly discuss various types of NLSMs, which are summarized in Fig. 1.

* pychang@phys.nthu.edu.tw

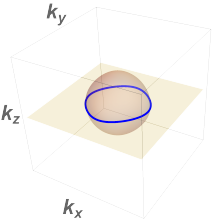
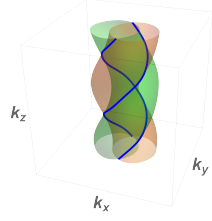
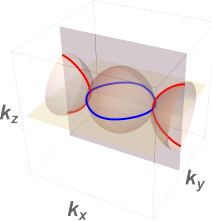
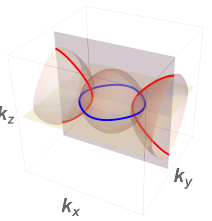
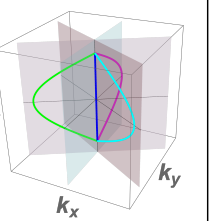
Nodal-line SM	Weyl-link SM	Nodal-chain SM	Hopf-link SM	Nexus SM
				
Chiral, mirror, \mathcal{PT} and other symmetries	Chiral symmetry	Mirror/glide symmetry	Mirror/glide symmetry	3-fold rotation symmetry
TlTaSe ₂ ^[8] ZrSiS ^[17] SnTaS ₂ ^[23] ZrSiSe ^[18] PbTaS ₂ ^{[15][68]} ZrSiTe ^[22] CaAgP ^[21] ZrGeSe ^[19] CaAgAs ^{[16][20]} Mg ₃ Bi ₂ ^{[38][39]} SrAs ₃ ^{[24][66]} CsTi ₃ Bi ₅ ^[40]		IrF ₄ ^{[44][47]} Ag ₂ BiO ₃ ^[50] Mg ₂ VO ₄ ^[46] FeIn ₂ S ₄ ^[49] MgCaN ₂ ^[48]	Co ₂ MnGa ^{[56][57]} Ba ₃ Si ₄ ^[48] MgSrSi ^[58]	Carbon honeycombs ^[54] WC ^[53]

FIG. 1. We summarize various types of NLSM, highlighting the nodal-line structures, symmetry constraints, and materials candidates.

A. NLSMs protected by symmetries

A simple NLSM can be described by an effective two-band $k \cdot p$ model

$$\mathcal{H}_{\mathbf{k}} = (k_x^2 + k_y^2 - \mu)\sigma_x + k_z\sigma_y, \quad (1)$$

where $\sigma_{\alpha=x,y,z}$ are Pauli matrices and μ is the chemical potential. The single-particle energy spectrum is $E_{\mathbf{k}}^{\pm} = \pm\sqrt{(k_x^2 + k_y^2 - \mu)^2 + k_z^2}$, with the nodal line is located on the $k_z = 0$ plane, as shown Fig. 1. The topological invariant associated with this nodal line is given by \mathbb{Z} , which can be computed as the winding number for a contour encircling the nodal line

$$\nu = \frac{i}{2\pi} \int_C \langle u_{\mathbf{k}}^- | du_{\mathbf{k}}^- \rangle, \quad (2)$$

where $|u_{\mathbf{k}}^-\rangle$ is the occupied state with energy $E_{\mathbf{k}}^-$. From Eq. (1), we can add a mass term $m\sigma_z$ to gapped out the nodal line. However, this mass term is forbidden if the system possesses chiral or mirror symmetries. I.e., $\mathcal{S} = \sigma_z$, $\mathcal{S}^\dagger \mathcal{H}_{\mathbf{k}} \mathcal{S} = -\mathcal{H}_{\mathbf{k}}$ or $\mathcal{M}_z = \sigma_y$, $\mathcal{M}_z^\dagger \mathcal{H}_{\mathbf{k}} \mathcal{M}_z = \mathcal{H}_{\bar{\mathbf{k}}}$ with $\bar{\mathbf{k}} = (\mathbf{k}_x, \mathbf{k}_y, -\mathbf{k}_z)$. We discuss the symmetry-protected nodal lines below.

a. *Mirror protected NLSM* For NLSM protected by the mirror symmetry, the nodal lines are located on the mirror plane ($k_z = 0, \pm\pi$). The nodal lines are formed by the band-degeneracy points. At the mirror plane, the band-degeneracy points possess two different mirror eigenvalues, preventing the degeneracy from being lifted. The topological invariant associated with a mirror protected nodal line is given by $M\mathbb{Z}$ [31].

b. *\mathcal{PT} protected NLSM* NLSMs can also be protected by the combination of parity \mathcal{P} and time-reversal \mathcal{T} symmetries. The \mathcal{PT} -protected nodal lines are characterized by a

\mathbb{Z}_2 topological invariant [11–13]. \mathcal{PT} symmetry enforces the Hamiltonian to be real. One can define the \mathbb{Z}_2 topological invariant by finding a one-dimensional line encircling the nodal line or a two-dimensional sphere enclosing it. Since these one-dimensional lines or two dimensional spheres correspond to real and gapped Hamiltonians, the \mathbb{Z}_2 topological classification is given by [32]

$$\pi_1 \left(\frac{O(M+N)}{O(M) \oplus O(N)} \right) = \pi_2 \left(\frac{O(M+N)}{O(M) \oplus O(N)} \right) = \mathbb{Z}_2. \quad (3)$$

The effective Hamiltonian is a four-band model

$$\mathcal{H}_{\mathbf{k}} = k_x\sigma_x + k_y\tau_y\sigma_y + k_z\sigma_z + m\tau_x\sigma_x, \quad (4)$$

where σ_i and τ_j are two sets of Pauli matrices. The nodal line is located on the $k_z = 0$ plane. The energy dispersion from Eq. (4) is $E_{\mathbf{k}} = \pm\sqrt{k_z^2 + (\sqrt{k_x^2 + k_y^2} \pm m)^2}$. By turning the mass term m , the nodal line cannot be annihilated by itself. I.e., the radius of the nodal line can only shrink to a point and cannot disappear by varying m .

c. *Nonsymmorphic symmetry protected NLSM* Nonsymmorphic symmetries such as glide mirror symmetry or screw rotation symmetry can protect the band touching points on the glide mirror plane or the screw rotation axis [11, 33–36]. We provide two examples of the nonsymmorphic symmetry-protected NLSMs below.

Glide mirror Let us consider the glide reflection $G_z = T_{(1/2, 0, 1/2)} M_z$. When we square the glide reflection operator, we get

$$\begin{aligned} G_z^2 &= T_{(1/2, 0, 1/2)} M_z T_{(1/2, 0, 1/2)} M_z \\ &= T_{(1, 0, 0)} M_z^2 = -T_{(1, 0, 0)} = -e^{-ik_x}. \end{aligned} \quad (5)$$

Here the minus sign is due to the half-integer character of the electron, meaning that the reflection square yields -1 . On the glide plane $k_z = 0, \pi$, the glide eigenvalues of the bands are $\pm ie^{-ik_x/2}$. Suppose the system exhibits time-reversal symmetry (TRS). The time-reversal invariant points (TRIP) on the glide plane must be double degenerate, forming the Kramers' pairs. The corresponding glide eigenvalues at two different TRIPs are $\pm i$ or ± 1 as shown in Fig. 2(a). The connectivity of bands along any path on the glide plane connecting two different TRIPs will exhibit hourglass structure, which guarantees a band crossing along the path. These band crossings will form a nodal-ring structure on the glide plane, referred to as a glide protected NLSM.

Screw rotation A similar analysis can be applied to screw rotations. Let us consider the two-fold screw rotation $C_x = T_{(1/2,1/2,0)}S_x$ where $S_x := (x, y, z) \rightarrow (x, -y, -z)$. When we square the screw rotation operator, we get

$$\begin{aligned} C_x^2 &= T_{(1/2,1/2,0)}S_x \\ &= T_{(1,0,0)}S_x^2 = -T_{(1,0,0)} = -e^{-ik_x}. \end{aligned} \quad (6)$$

There are four screw rotation lines $(k_x, 0, 0)$, $(k_x, 0, \pi)$, $(k_x, \pi, 0)$, and (k_x, π, π) . The bands along these lines will have the screw eigenvalues $\pm ie^{-ik_x/2}$. Through a similar analysis as before, in the presence of TRS, there is a hourglass structure exists between two TRIPs, which guarantees the presence of Weyl points along the $(k_x, 0, 0)$ axis. Interestingly, if there are two other two-fold crew rotations $C_y = T_{(0,1/2,1/2)}S_y$ with $S_y := (x, y, z) \rightarrow (-x, y, -z)$ and $C_z = T_{(1/2,0,1/2)}S_z$ with $S_y := (x, y, z) \rightarrow (-x, -y, z)$, TRS combined with this screw rotation symmetries will enforce the Kramers degeneracy on the boundaries of the Brillouin zone. For example, along the line (k_x, π, π) , we can consider the combination of TRS and screw rotation symmetries TC_y and TC_z . When we square these combined symmetries

$$\begin{aligned} (TC_y)^2 &= T^2C_y^2 = e^{-ik_y} = -1, \quad k_y = \pi, \\ (TC_z)^2 &= T^2C_z^2 = e^{-ik_z} = -1, \quad k_z = \pi. \end{aligned} \quad (7)$$

These combined antiunitary operators squaring to minus one indicate that along the (k_x, π, π) axis, the bands must form Kramers' pairs [see Fig. 2(b)].

d. Pseudospin Vortex Ring SMs Beside symmetry-protected nodal lines, one can also consider the nodal line as vortex line, where the pseudospin texture around the nodal line forms a toroidal vector field around its axis [14]. The effective two-band Hamiltonian is given by

$$\begin{aligned} \mathcal{H}_k &= -\frac{1}{m_z}k_xk_z\sigma_x - \frac{1}{m_z}k_yk_z\sigma_y \\ &\quad + \left(\frac{1}{m_r}(k_x^2 + k_y^2 - k_z^2 - k_0^2)\right), \end{aligned} \quad (8)$$

where the nodal line forms a ring on the $k_z = 0$ plane, k_0 sets the radius of the ring, and $m_{r/z}$ sets the Fermi velocities. The pseudospin texture can be understood from the following

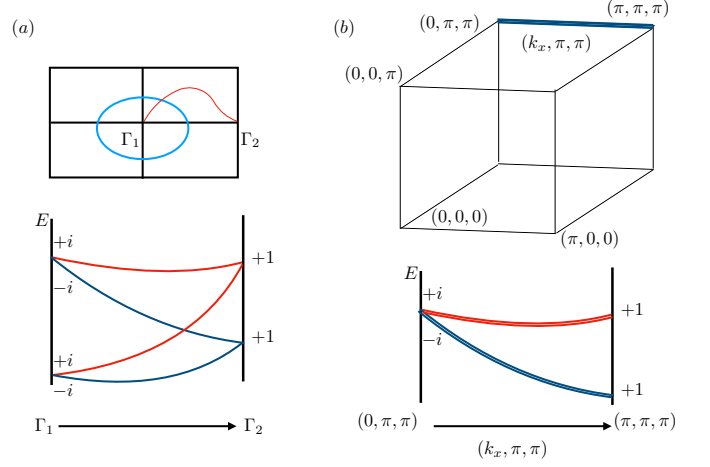


FIG. 2. NLSMs protected by non-symmorphic symmetries (glide reflection or screw rotation): (a) **Glide Mirror Protections:** (Upper panel) Any red path on the glide plane connecting two time-reversal invariant points Γ_1 and Γ_2 will host a degenerate point. Connecting all such degenerate points forms a nodal line (blue circle). (Lower panel) The glide eigenvalues $\pm ie^{-ik_x/2}$ at two different time-reversal invariant points Γ_1 and Γ_2 are $\pm i$ and ± 1 are switched. I.e., $\pm i$ at Γ_1 becomes $+1$ or -1 at Γ_2 . The energy spectrum exhibits an hourglass structure and giving rise to a degenerate point. (b) **Screw Rotation Protection:** The nodal line (which is double degenerate) lies along the screw rotation axis (k_x direction). Here additional symmetries (TC_y and TC_z), when combined with time-reversal and screw rotations, lead to Kramers' pairs along the (k_x, π, π) line.

procedure. First, for a fixed k_y plane that intersects with the nodal ring, there are two Dirac points. Each of the Dirac point can be expressed as $\mathcal{H}_k = -k_z\sigma_x + k_x\sigma_z$. The pseudospin winds a 2π angle along a trajectory that encircles the Dirac point. Hence this nodal ring can be viewed as a vortex ring.

e. Type-I/II/III NLSMs Nodal lines can be classified into three types based on their differing dispersions [37]. This classification can be obtained using a simple two-band model at the Γ point

$$\begin{aligned} \mathcal{H}_k &= \frac{1}{2}((A_1 + A_2)k_x^2 + (B_1 + B_2)k_y^2 + \Delta) \mathbb{I} \\ &\quad + \frac{1}{2}((A_1 - A_2)k_x^2 + (B_1 - B_2)k_y^2 - \Delta) \sigma_z + Ck_z\sigma_y, \end{aligned} \quad (9)$$

where A_1, A_2, B_1, B_2, C and Δ are tuning parameters that can be determined from the *ab initio* calculation. For simplicity, we set $C = 1$.

- Type-I: When $A_1, B_1 > 0, A_2, B_2 < 0$, the NLSM is classified as type-I, as shown in Fig. 3(a).
- Type-II: When $A_1, A_2, B_1, B_2 > 0$ or $A_1, A_2, B_1, B_2 < 0$, the NLSM is classified as type-II, as shown in Fig. 3(b).
- Type-III: When $A_1, A_2, B_1 > 0, B_2 < 0$, or $B_1, B_2, A_2 < 0, A_1 > 0$, the NLSM is classified as type-III, as shown in Fig. 3(c).

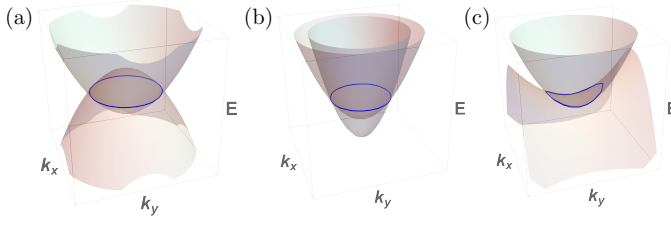


FIG. 3. Classification of energy dispersions near the nodal line: (a) Type I, (b) Type II, and (c) Type III.

These different dispersions can strongly influence the transport properties, as we will discuss the Landau level spectrum in Sec. III A. Most of the NLSMs are belong to type-I. Mg₃Bi₂ is a candidate material for a type-II NLSM [38, 39]. CsTi₃Bi₅ is a candidate material for a type-III NLSM [40].

B. Nodal-link/Weyl-link SMs

For a two-band model with chiral (sublattice symmetry) $\mathcal{S}\mathcal{H}(\mathbf{k})\mathcal{S}^{-1} = -\mathcal{H}(\mathbf{k})$, where $\mathcal{H}(\mathbf{k}) = f(\mathbf{k})\sigma_x + g(\mathbf{k})\sigma_y$, one can find two periodic functions $f(\mathbf{k})$ and $g(\mathbf{k})$ such that the nodal lines linked to each other. For simplicity, we consider

$$\begin{aligned} f(\mathbf{k}) &= (1 + \cos k_x + \cos k_y), \\ g(\mathbf{k}) &= [\sin(nk_z) + \cos(nk_z)] \sin k_x \\ &\quad - [\sin(nk_z) - \cos(nk_z)] \sin k_y, \end{aligned} \quad (10)$$

where $n \in \mathbb{Z}$. This integer n determines the linking number. For $n = 0$, there are two straight nodal lines extending along the k_z -direction. For $n = \pm 1$, these two nodal lines form a helical structure along the k_z -direction, which is equivalent to the Hopf link, as shown in Fig. 1.

The linking number associated with the nodal lines can be connected to the Chern-Simons theory. From Eq. 2, the winding number can be repressed in terms of the Berry connection $\mu = \frac{1}{2\pi} \oint_C a$, where the Berry connection is $a = i\langle u_{\mathbf{k}} | du_{\mathbf{k}} \rangle$. The Chern-Simons 3-form is defined as

$$\theta = \frac{1}{4\pi} \int_{BZ} \text{Tr}(a \wedge da - \frac{2i}{3} a \wedge a \wedge a). \quad (11)$$

This Chern-Simons 3-form describes the electromagnetic response of the three-dimensional topological insulator, where

the θ angle is quantized to be π in the topological phase and is zero in the trivial phase due to the time-reversal symmetry. For nodal-link/Weyl-link SMs, the Chern-Simons 3-form is related to the linking number

$$\frac{1}{4\pi} \int_{BZ} a \wedge da = \pi \sum_{i,j} \nu_i \nu_j N(\mathcal{L}_i, \mathcal{L}_j), \quad (12)$$

where ν_i is the vorticity associated with the nodal lines, and $N(\mathcal{L}_i, \mathcal{L}_j)$ is the Gauss linking integral,

$$N(\mathcal{L}_i, \mathcal{L}_j) = \frac{1}{4\pi} \oint_{\mathcal{L}_i} dx^i \oint_{\mathcal{L}_j} dy^j \epsilon_{ijk} \frac{(x-y)^k}{|x-y|^3}, \quad (13)$$

which determines the number of times two loops \mathcal{L}_i and \mathcal{L}_j linked with each other. Similar constructions of Nodal-link/Weyl-link SMs are discussed in Refs. [26, 41–43].

C. Nodal-chain SMs

The nodal-chain SM was first introduced in Ref. [44]. In this phase, the nodal lines form a chain-like structure where all the nodal lines are connected to each others. The first criterion for hosting a nodal-chain SM phase is the existence of the non-symmorphic symmetry-protected NLSMs (specifically, glide mirror), as discussed in Sec. II A 0c. The system also needs to possess two inequivalent glide planes, with time-reversal invariant points (TRIPs) located at the intersections of these planes. The final criterion is that the intersection of the nodal loops forming the chain much belong to the two-dimensional representations at the TRIPs. The chain configuration is illustrated in Fig. 1. Similar nodal-chain SMs are also discussed in Refs. [45–50]

D. Nexus fermion, triplet points, and their nodal networks

Triplet degenerate points that can be visualized as the terminal points of several nodal lines are referred to as the Nexus points [51–53]. These Nexus points can be protected by three-fold rotation symmetry, and the effective $k \cdot p$ model can be written as

$$\mathcal{H}(\mathbf{k}) = \begin{pmatrix} A_1(k_x^2 + k_y^2) + B_1 \cos k_z + C_1 & \alpha(k_x + ik_y) \sin k_z + \beta(k_x - ik_y)^2 & D(k_x - ik_y) \\ \alpha(k_x - ik_y) \sin k_z + \beta(k_x + ik_y)^2 & A_1(k_x^2 + k_y^2) + B_1 \cos k_z + C_1 & -D(k_x + ik_y) \\ D(k_x + ik_y) & D(k_x - ik_y) & A_2(k_x^2 + k_y^2) + B_2 \cos k_z + C_2 \end{pmatrix}. \quad (14)$$

For $\alpha = 0$, the Hamiltonian exhibits a six-fold rotation sym-

metry. For $\alpha \neq 0$, the six-fold rotation symmetry is bro-

ken down to a three-fold rotation symmetry. The triplet point (three-fold degeneracy) is located on the rotation axis. Besides the three-fold rotation symmetry, there are three additional mirror planes, each hosting nodal lines. These nodal lines merge at the intersection of these mirror planes, i.e., at the rotation axis. The merging point is the Nexus point, where the first two-fold degenerate nodal-line (formed by the first and the second bands) meets the second two-fold degenerate nodal-line (formed by the second and the third bands). Therefore, the merging point is a three-fold degeneracy point.

The first two-fold degenerate nodal-line and the second two-fold degenerate nodal-line, together with their merging points (Nexus points) arrange themselves as a chain-like structure, referred to as the Nexus network [54]. It should be noted that this network structure differs from nodal-chain SMs. The merging points of the nodal-chain SMs are still two-fold degenerate, unlike the Nexus network where the merging points are three-fold degenerate.

We can also consider another variance of the nodal network by further breaking the rotation symmetry. For the triplet point that is protect by C_4 screw rotations [55], breaking the C_4 screw rotations can lead to the splitting of the triple point into two-fold degenerate points. The first two-fold degenerate nodal-line and the second two-fold degenerate nodal-line do not merge and become two individual nodal loops on their corresponding mirror planes. These nodal loops can form non-trivial link (Hopf link) and thus form Hopf-link networks [26, 45, 55–59].

III. ELECTROMAGNETIC RESPONSE

The electromagnetic response in these NLSMs is very rich due to their anisotropy and tunability. Similar to other semimetals, such as graphene and Weyl semimetals, the transport properties under an external magnetic field are strongly related to the topological nature of their nodal structures. Furthermore, the optical conductivity can be sensitive to both their band dispersions and nodal structures. As discussed in the previous section, nodal structures are related to crystal symmetry and can be broken by applying external strain or fields. Additionally, the dispersion can be highly anisotropic. All these properties suggest a huge potential for applications stemming from their electromagnetic response.

A. Landau level

For NLSMs in three dimensions, consider a given two-dimensional slice embedded in the 3D Brillouin zone. There can be several gapless points where this two-dimensional slice intersects with the nodal lines. These gapless points within the two-dimensional slice are analogous to the Dirac cones found in a graphene sheet. When an external magnetic field is applied perpendicular to graphene, a zeroth Landau level appears at zero energy. For NLSMs subjected to an external magnetic field, one can visualize the perpendicular 2D

slices as graphene-like systems with Dirac cones, where zeroth Landau levels are associated with each of these graphene-like slices. These zeroth Landau levels are linked to forming a dispersionless band [25, 26]. These flat bands strongly depend on how the two-dimensional slices (perpendicular to the field) intersect with the nodal lines. In principle, by applying Landau level spectroscopy with varying field directions, one can map out the nodal-line structure of an NLSM.

B. Optical conductivity/permittivity, and hyperbolic polariton

The optical conductivity can be directly computed from the Kubo formula

$$\sigma_{\alpha\beta}(\omega) = \frac{i\hbar}{V} \sum_{m,n,\sigma} \frac{f_{n\sigma} - f_{m\sigma}}{E_{m\sigma} - E_{n\sigma}} \frac{\langle \psi_{n\sigma} | J_\alpha | \psi_{m\sigma} \rangle \langle \psi_{m\sigma} | J_\beta | \psi_{n\sigma} \rangle}{\hbar(\omega + i\Gamma) + E_{n\sigma} - E_{m\sigma}}, \quad (15)$$

where $\alpha, \beta = x, y, z$, $\sigma = \uparrow, \downarrow$, m, n are the band labels, $f_{m\sigma} = (1 + e^{(E_{m\sigma} - \mu)/k_B T})^{-1}$, T is the temperature, μ is the chemical potential, $J_\alpha = \hbar^{-1} \partial_{k_\alpha} \mathcal{H}_k$ is the current operator, and Γ is the phenomenological decay term.

If the nodal-line structure is highly anisotropic, it can give rise to a strong anisotropy optical conductivity in different direction. For example, for a nodal-line structure shaped like a ring at the $x - y$ plane, as shown in Fig. 3, the optical conductivity tensor can be highly anisotropic, meaning $\sigma_{xx} = \sigma_{yy} \neq \sigma_{zz}$. It can lead to opposite signs of the dielectric permittivity tensor ϵ_{xx} and ϵ_{zz} . As discussed in Ref. [60], this opposite sign of dielectric permittivity tensor implies that the optical response is plasmonic in one direction and dielectric in other directions. The associated polariton dispersion then becomes hyperbolic and is referred to as the hyperbolic polaritons.

IV. CORRELATIONS

A. magnetization

The bulk-boundary correspondence of NLSMs is characterized by the surface drumhead states, where nearly flat bands emerge on the surface from the bulk nodal lines projected onto the surface Brillouin zone. The dispersions of these drumhead states are nearly flat, which imply strong interaction effects. These interactions can lead to several symmetry-breaking orders, including the magnetization (time-reversal symmetry breaking), the charge-density-wave (translation symmetry breaking), and superconductivity ($U(1)$ symmetry breaking).

The type of magnetization orders depends on the details of the interaction. In Ref. [61], the author consider the onsite (U) and the nearest neighbor (V) repulsive interactions, and found that the surface magnetic orders could be either antiferromagnetic (U dominated) or ferromagnetic (V dominated). These surface magnetic orders can lead to surface magnons, whose spectra can be tuned by the thickness of the slab geometry [62]. Besides surface magnetic orders, bulk interactions can also drive the systems into a nodal-line semimetallic

phase. In particular, the Hund's coupling between the local moments with the itinerant electron spins can lead to nodal-line semimetallic phases [63, 64].

B. superconductivity

Superconductivity has been reported in several NLSMs [65–70]. Although the topological properties of the NLSMs in their normal states may transition to their superconducting states, most experimental observations cannot confirm the existence of topological superconductivity. Nevertheless, unconventional superconductivity has been reported, including:

- Multi-gap structures in CaSb₂ [71, 72].
- Time-reversal-symmetry breaking of the superconducting states in LaNiGa₂ [73], LaNiSi, LaPtSi, and LaPtGe [74].
- Anisotropic gap structure in SnTaS₂ [75] and In_xTaS₂ [76].
- *s + ip* superconductivity in TRuSi (*T* being transition metals) [77].
- Coexistence of topological surface states and bulk superconductivity in PbTaSe₂ [78].

Theoretical models for studying the superconductivity in NLSMs often begin with the torus-like Fermi surface [79–86]. These torus-like Fermi surfaces differ from the conventional spherical or cylindrical Fermi surfaces, where the time-reversal-symmetry breaking superconducting states are preferred [79–81]. Topological superconductivity is also proposed in these theoretical models, including the crystalline, fragile, and higher-order topological superconductors [82, 83, 86], as well as nodal superconductivity [85]. Similar to the spontaneous symmetry-breaking orders on the drumhead surface states, surface superconductivity can arise and has been reported for CaAg_{1-x}Pd_xP [87].

C. Kondo effects

The Kondo effect describes the interaction of free conduction electrons with magnetic moments in materials, which can lead to a strong renormalization of effective mass and band dispersion. These magnetic moments are usually formed by localized *f*-electrons. If these *f*-electrons are arranged into a lattice structure (i.e., a Kondo lattice), the corresponding dispersion becomes flat. The effective Hamiltonian is the Anderson lattice model

$$H = \sum_{i,j,\sigma,\sigma'} \Psi_{i\sigma}^\dagger \mathcal{H}_{ij,\sigma\sigma'} \Psi_{j\sigma'} + U \sum_i n_{if\uparrow} n_{if\downarrow}, \quad (16)$$

where

$$\mathcal{H}_{ij,\sigma\sigma'} = \begin{pmatrix} (-t_{i,j}^c - \mu^c \delta_{ij}) \delta_{\sigma\sigma'} & V_{\sigma\sigma'}(\mathbf{R}_i - \mathbf{R}_j) \\ V_{\sigma\sigma'}(\mathbf{R}_i - \mathbf{R}_j) & (-t_{i,j}^f - \mu^f \delta_{ij}) \delta_{\sigma\sigma'} \end{pmatrix}. \quad (17)$$

Here $t_{i,j}^{c/f}$ is the hopping terms for conduction/*f*-electrons, $\mu^{c/u}$ is the chemical potential of conduction/*f*-electrons, $V_{\sigma\sigma'}(\mathbf{R}_i - \mathbf{R}_j)$ represents the hybridization between conduction and *f*-electrons, $\Psi_{i\sigma}^\dagger = (c_{i\sigma}^\dagger, f_{i\sigma}^\dagger)$ with $c_{i\sigma}^\dagger$ and $f_{i\sigma}^\dagger$ are the creation operators for conduction and *f*-electrons.

One can derive a simple model of the above Hamiltonian under the self-consistent mean-field approach in the large *U* limit [88]. The mean-field Hamiltonian takes the form $H = \sum_{\mathbf{k}} \Psi^\dagger(\mathbf{k}) \mathcal{H}(\mathbf{k}) \Psi(\mathbf{k}) + \mathcal{N}_s \lambda(|b|^2 - Q)$ with

$$\mathcal{H}(\mathbf{k}) = \begin{pmatrix} \epsilon_c(\mathbf{k}) - \mu & \sum_j V_j \sigma_j \sin k_j \\ \sum_j V_j \sigma_j \sin k_j & \epsilon_f(\mathbf{k}) + \lambda \end{pmatrix} + \begin{pmatrix} 0 & W_0 + i\vec{W} \cdot \vec{\sigma} \\ W_0 - i\vec{W} \cdot \vec{\sigma} & 0 \end{pmatrix}. \quad (18)$$

Here $V_i = v_i b$ and $W_i = w_i b$ are the renormalized hybridization terms with *b* being the slave boson projection amplitude. The *f*-electron hopping amplitude is renormalized as $\tilde{t}^f = b^2 t^f$. For simplicity, we take the dispersion of the conduction electrons as $\epsilon_c(\mathbf{k}) = -2 \sum_i t_i \cos k_i$ and $\epsilon_f(\mathbf{k}) = \alpha \epsilon_c(\mathbf{k})$. Under the mean-field constraint $Q = n_f + b^2$, we introduce the constraint field λ . Here Q is the local conserved charge associated with the slave boson approach in the infinite *U* limit, and it is taken to be $Q = 1$. \mathcal{N}_s is the total number of sites. When $\vec{W} = 0$ with non-vanishing W_0 , the system exhibit two nodal rings protected by the chiral symmetry. The dispersion near the nodal rings are strongly renormalized by the *f*-electrons.

Beyond this simple model, other topological nodal-line "Kondo" semimetals have been reported including Ce₃Pd₃Bi₄ [89], CePt₂Si₂ [90], Ce₂Au₃In₅ [91], and antiferromagnetic CeCo₂P₂ [92].

V. CONCLUSION AND OUTLOOK

We review different types of NLSMs whose nodal structures depend on their underlying crystalline symmetries. The electromagnetic responses of these NLSMs are highly sensitive to their nodal structures, providing platforms for transport and optical applications. The correlation effects in these materials are rich, giving rise to magnetic orders, unconventional superconductivity, and heavy fermion physics. Furthermore, several promising future directions for NLSMs could lead to interesting material properties and potential applications:

- Heterostructures: The surface drumhead states in NLSMs offer a platform to engineer interesting correlated phases through heterostructures. For instance, exotic magnetic orders can emerge from interacting surface drumhead states. Topological superconductivity, arising from the intertwining of magnetism and superconductivity, may also be realized in NLSM-superconducting heterostructures. Recently, unconventional Andreev reflections in such systems have been explored in Refs [93, 94].

- Quantum geometry: Recent research has focused on the quantum geometric origin of the non-linear Hall effect (NLHE) [95–104]. The quantum geometric contribution to the NLHE can be significantly enhanced by (nearly gapped) Dirac/Weyl cones and nodal lines [102, 105, 106]. For NLSMs, their three-dimensional nodal-line structures are expected to lead to strong anisotropic NLHE, making them an interesting area for investigation.
- Terahertz (THz) application: Operating optoelectronics (e.g., lasers, modulators, or photodetectors) in the THz regime presents a challenge for conventional electronic materials. To overcome this limitation, it has been proposed that (narrow-gap) semimetals can provide suitable platforms for THz devices [107–110].

Current research primarily focuses on graphene, Dirac semimetals, and the surface states of topological insulators [110]. Investigating the potential application of NLSMs in THz devices would be highly desirable.

ACKNOWLEDGMENTS

P.-Y. C. acknowledges support from the National Science and Technology Council of Taiwan under Grants No. NSTC 113-2112-M-007-019, 114-2918-I-007-015, and the support from Yukawa Institute for Theoretical Physics, Kyoto University, RIKEN Center for Interdisciplinary Theoretical and Mathematical Sciences, and National Center for Theoretical Sciences, Physics Division.

-
- [1] M. Z. Hasan and C. L. Kane, Colloquium: Topological insulators, *Rev. Mod. Phys.* **82**, 3045 (2010).
- [2] X.-L. Qi and S.-C. Zhang, Topological insulators and superconductors, *Rev. Mod. Phys.* **83**, 1057 (2011).
- [3] Q. Yan, H. Li, H. Jiang, and X. Xie, Towards dissipationless topotronics, *Materials Today Quantum* **5**, 100023 (2025).
- [4] N. P. Armitage, E. J. Mele, and A. Vishwanath, Weyl and dirac semimetals in three-dimensional solids, *Rev. Mod. Phys.* **90**, 015001 (2018).
- [5] A. A. Burkov, M. D. Hook, and L. Balents, Topological nodal semimetals, *Phys. Rev. B* **84**, 235126 (2011).
- [6] S. Matsuura, P.-Y. Chang, A. P. Schnyder, and S. Ryu, Protected boundary states in gapless topological phases, *New Journal of Physics* **15**, 065001 (2013).
- [7] R. Yu, H. Weng, Z. Fang, X. Dai, and X. Hu, Topological node-line semimetal and dirac semimetal state in antiperovskite cu_3PdN , *Phys. Rev. Lett.* **115**, 036807 (2015).
- [8] G. Bian, T.-R. Chang, H. Zheng, S. Velury, S.-Y. Xu, T. Neupert, C.-K. Chiu, S.-M. Huang, D. S. Sanchez, I. Belopolski, N. Alidoust, P.-J. Chen, G. Chang, A. Bansil, H.-T. Jeng, H. Lin, and M. Z. Hasan, Drumhead surface states and topological nodal-line fermions in lttase_2 , *Phys. Rev. B* **93**, 121113 (2016).
- [9] Y.-H. Chan, C.-K. Chiu, M. Y. Chou, and A. P. Schnyder, ca_3p_2 and other topological semimetals with line nodes and drumhead surface states, *Phys. Rev. B* **93**, 205132 (2016).
- [10] Y. X. Zhao and Z. D. Wang, Topological classification and stability of fermi surfaces, *Phys. Rev. Lett.* **110**, 240404 (2013).
- [11] C. Fang, Y. Chen, H.-Y. Kee, and L. Fu, Topological nodal line semimetals with and without spin-orbital coupling, *Phys. Rev. B* **92**, 081201 (2015).
- [12] C. Fang, H. Weng, X. Dai, and Z. Fang, Topological nodal line semimetals*, *Chinese Physics B* **25**, 117106 (2016).
- [13] Y. X. Zhao and Y. Lu, pt -symmetric real dirac fermions and semimetals, *Phys. Rev. Lett.* **118**, 056401 (2017).
- [14] L.-K. Lim and R. Moessner, Pseudospin vortex ring with a nodal line in three dimensions, *Phys. Rev. Lett.* **118**, 016401 (2017).
- [15] J.-P. Sun, Topological nodal line semimetal in non-centrosymmetric pbta_2 *, *Chinese Physics Letters* **34**, 077101 (2017).
- [16] X.-B. Wang, X.-M. Ma, E. Emmanouilidou, B. Shen, C.-H. Hsu, C.-S. Zhou, Y. Zuo, R.-R. Song, S.-Y. Xu, G. Wang, L. Huang, N. Ni, and C. Liu, Topological surface electronic states in candidate nodal-line semimetal caagas, *Phys. Rev. B* **96**, 161112 (2017).
- [17] R. Singha, A. K. Pariari, B. Satpati, and P. Mandal, Large nonsaturating magnetoresistance and signature of nondegenerate dirac nodes in zrsis, *Proceedings of the National Academy of Sciences* **114**, 2468 (2017), <https://www.pnas.org/doi/pdf/10.1073/pnas.1618004114>.
- [18] H. Pan, B. Tong, J. Yu, J. Wang, D. Fu, S. Zhang, B. Wu, X. Wan, C. Zhang, X. Wang, and F. Song, Three-dimensional anisotropic magnetoresistance in the dirac node-line material zrsise, *Scientific Reports* **8**, 9340 (2018).
- [19] L. Guo, T.-W. Chen, C. Chen, L. Chen, Y. Zhang, G.-Y. Gao, J. Yang, X.-G. Li, W.-Y. Zhao, S. Dong, and R.-K. Zheng, Electronic transport evidence for topological nodal-line semimetals of zrgese single crystals, *ACS Applied Electronic Materials* **1**, 869 (2019), <https://doi.org/10.1021/acsaelm.9b00061>.
- [20] H. T. Hirose, T. Terashima, T. Wada, Y. Matsushita, Y. Okamoto, K. Takenaka, and S. Uji, Real spin and pseudospin topologies in the noncentrosymmetric topological nodal-line semimetal caagas, *Phys. Rev. B* **101**, 245104 (2020).
- [21] Y. Okamoto, K. Saigusa, T. Wada, Y. Yamakawa, A. Yamakage, T. Sasagawa, N. Katayama, H. Takatsu, H. Kageyama, and K. Takenaka, High-mobility carriers induced by chemical doping in the candidate nodal-line semimetal caagp, *Phys. Rev. B* **102**, 115101 (2020).
- [22] B. A. Stuart, S. Choi, J. Kim, L. Muechler, R. Queiroz, M. Oudah, L. M. Schoop, D. A. Bonn, and S. A. Burke, Quasiparticle interference observation of the topologically non-trivial drumhead surface state in zrsite, *Phys. Rev. B* **105**, L121111 (2022).
- [23] W. Gao, M. Zhu, D. Chen, X. Liang, Y. Wu, A. Zhu, Y. Han, L. Li, X. Liu, G. Zheng, W. Lu, and M. Tian, Evidences of topological surface states in the nodal-line semimetal sntas2 nanoflakes, *ACS Nano* **17**, 4913 (2023), pMID: 36802534, <https://doi.org/10.1021/acsnano.2c11932>.
- [24] J. Jeon, J. Jang, H. Kim, T. Park, D. Kim, S. Moon, J. S. Kim, J. H. Shim, H. Min, and E. Choi, Optical transitions of a single nodal ring in sras_3 : Radially and axially resolved characteri-

- zation, *Phys. Rev. Lett.* **131**, 236903 (2023).
- [25] J.-W. Rhim and Y. B. Kim, Landau level quantization and almost flat modes in three-dimensional semimetals with nodal ring spectra, *Phys. Rev. B* **92**, 045126 (2015).
- [26] P.-Y. Chang and C.-H. Yee, Weyl-link semimetals, *Phys. Rev. B* **96**, 081114 (2017).
- [27] R. Yu, Z. Fang, X. Dai, and H. Weng, Topological nodal line semimetals predicted from first-principles calculations, *Frontiers of Physics* **12**, 127202 (2017).
- [28] M.-X. Yang, W. Luo, and W. C. and, Quantum transport in topological nodal-line semimetals, *Advances in Physics: X* **7**, 2065216 (2022), <https://doi.org/10.1080/23746149.2022.2065216>.
- [29] H. Park, W. Gao, X. Zhang, and S. S. Oh, Nodal lines in momentum space: topological invariants and recent realizations in photonic and other systems, *Nanophotonics* **11**, 2779 (2022).
- [30] S.-Y. Yang, H. Yang, E. Derunova, S. S. P. Parkin, B. Yan, and M. N. A. and, Symmetry demanded topological nodal-line materials, *Advances in Physics: X* **3**, 1414631 (2018), <https://doi.org/10.1080/23746149.2017.1414631>.
- [31] C.-K. Chiu and A. P. Schnyder, Classification of reflection-symmetry-protected topological semimetals and nodal superconductors, *Phys. Rev. B* **90**, 205136 (2014).
- [32] A. Hatcher, *Algebraic Topology*, Algebraic Topology (Cambridge University Press, 2002).
- [33] S. M. Young and C. L. Kane, Dirac semimetals in two dimensions, *Phys. Rev. Lett.* **115**, 126803 (2015).
- [34] B.-J. Yang, T. A. Bojesen, T. Morimoto, and A. Furusaki, Topological semimetals protected by off-centered symmetries in nonsymmorphic crystals, *Phys. Rev. B* **95**, 075135 (2017).
- [35] R. Takahashi, M. Hirayama, and S. Murakami, Spinless hourglass nodal-line semimetals, *Phys. Rev. B* **96**, 155206 (2017).
- [36] A. Furusaki, Weyl points and dirac lines protected by multiple screw rotations, *Science Bulletin* **62**, 788 (2017).
- [37] Y. Gao, Y. Chen, Y. Xie, P.-Y. Chang, M. L. Cohen, and S. Zhang, A class of topological nodal rings and its realization in carbon networks, *Phys. Rev. B* **97**, 121108 (2018).
- [38] X. Zhang, L. Jin, X. Dai, and G. Liu, Topological type-ii nodal line semimetal and dirac semimetal state in stable kagome compound mg3bi2, *The Journal of Physical Chemistry Letters* **8**, 4814 (2017), pMID: 28927265, <https://doi.org/10.1021/acs.jpclett.7b02129>.
- [39] T.-R. Chang, I. Pletikosic, T. Kong, G. Bian, A. Huang, J. Dendlinger, S. K. Kushwaha, B. Sinkovic, H.-T. Jeng, T. Valla, W. Xie, and R. J. Cava, Realization of a type-ii nodal-line semimetal in mg3bi2, *Advanced Science* **6**, 1800897.
- [40] J. Yang, X. Yi, Z. Zhao, Y. Xie, T. Miao, H. Luo, H. Chen, B. Liang, W. Zhu, Y. Ye, J.-Y. You, B. Gu, S. Zhang, F. Zhang, F. Yang, Z. Wang, Q. Peng, H. Mao, G. Liu, Z. Xu, H. Chen, H. Yang, G. Su, H. Gao, L. Zhao, and X. J. Zhou, Observation of flat band, dirac nodal lines and topological surface states in kagome superconductor csti3bi5, *Nature Communications* **14**, 4089 (2023).
- [41] W. Chen, H.-Z. Lu, and J.-M. Hou, Topological semimetals with a double-helix nodal link, *Phys. Rev. B* **96**, 041102 (2017).
- [42] Z. Yan, R. Bi, H. Shen, L. Lu, S.-C. Zhang, and Z. Wang, Nodal-link semimetals, *Phys. Rev. B* **96**, 041103 (2017).
- [43] M. Ezawa, Topological semimetals carrying arbitrary hopf numbers: Fermi surface topologies of a hopf link, solomon's knot, trefoil knot, and other linked nodal varieties, *Phys. Rev. B* **96**, 041202 (2017).
- [44] T. Bzdušek, Q. Wu, A. Rüegg, M. Sigrist, and A. A. Soluyanov, Nodal-chain metals, *Nature* **538**, 75 (2016).
- [45] J. Cai, Y. Xie, P.-Y. Chang, H.-S. Kim, and Y. Chen, Nodal-chain network, intersecting nodal rings and triple points co-existing in nonsymmorphic ba3si4, *Phys. Chem. Chem. Phys.* **20**, 21177 (2018).
- [46] H. Zhang, X. Zhang, T. He, X. Dai, Y. Liu, G. Liu, L. Wang, and Y. Zhang, Three-dimensional weyl hourglass networks in the nonsymmorphic half-metal mg₂vo₄, *Phys. Rev. B* **102**, 155116 (2020).
- [47] C. Shang, O. Ganter, N. Heinsdorf, and S. M. Winter, irf₄: From tetrahedral compass model to topological semimetal, *Phys. Rev. B* **107**, 125111 (2023).
- [48] H. Wu, D.-S. Ma, and B. Fu, Hybrid nodal-chain semimetal with emergent flat band in mgcan2, *New Journal of Physics* **25**, 033005 (2023).
- [49] J. Liu, Y. Wang, X. Dong, J. Yang, S. Zhang, M. Lyu, B. Wang, H. Wei, S. Wang, E. Liu, and B. Shen, Topological nodal chains and transverse transport in the centrosymmetric ferromagnetic semimetal FeIn₂S₄, *Phys. Rev. B* **109**, 235144 (2024).
- [50] B. Fu, X. Fan, D. Ma, C.-C. Liu, and Y. Yao, Hourglasslike nodal net semimetal in ag₂bio₃, *Phys. Rev. B* **98**, 075146 (2018).
- [51] T. T. Heikkilä and G. E. Volovik, Nexus and dirac lines in topological materials, *New Journal of Physics* **17**, 093019 (2015).
- [52] T. Hyart and T. T. Heikkilä, Momentum-space structure of surface states in a topological semimetal with a nexus point of dirac lines, *Phys. Rev. B* **93**, 235147 (2016).
- [53] G. Chang, S.-Y. Xu, S.-M. Huang, D. S. Sanchez, C.-H. Hsu, G. Bian, Z.-M. Yu, I. Belopolski, N. Alidoust, H. Zheng, T.-R. Chang, H.-T. Jeng, S. A. Yang, T. Neupert, H. Lin, and M. Z. Hasan, Nexus fermions in topological nonsymmorphic crystalline metals, *Scientific Reports* **7**, 1688 (2017).
- [54] Y. Chen, Y. Xie, Y. Gao, P.-Y. Chang, S. Zhang, and D. Vanderbilt, Nexus networks in carbon honeycombs, *Phys. Rev. Mater.* **2**, 044205 (2018).
- [55] Y. Xie, J. Cai, J. Kim, P.-Y. Chang, and Y. Chen, Hopf-chain networks evolved from triple points, *Phys. Rev. B* **99**, 165147 (2019).
- [56] I. Belopolski, K. Manna, D. S. Sanchez, G. Chang, B. Ernst, J. Yin, S. S. Zhang, T. Cochran, N. Shumiya, H. Zheng, B. Singh, G. Bian, D. Multer, M. Litskevich, X. Zhou, S.-M. Huang, B. Wang, T.-R. Chang, S.-Y. Xu, A. Bansil, C. Felser, H. Lin, and M. Z. Hasan, Discovery of topological weyl fermion lines and drumhead surface states in a room temperature magnet, *Science* **365**, 1278 (2019), <https://www.science.org/doi/10.1126/science.aav2327>.
- [57] I. Belopolski, G. Chang, T. A. Cochran, Z.-J. Cheng, X. P. Yang, C. Hugelmeyer, K. Manna, J.-X. Yin, G. Cheng, D. Multer, M. Litskevich, N. Shumiya, S. S. Zhang, C. Shekhar, N. B. M. Schröter, A. Chikina, C. Polley, B. Thagarajan, M. Leandersson, J. Adell, S.-M. Huang, N. Yao, V. N. Strocov, C. Felser, and M. Z. Hasan, Observation of a linked-loop quantum state in a topological magnet, *Nature* **604**, 647 (2022).
- [58] J. Lian, L. Yu, Q.-F. Liang, J. Zhou, R. Yu, and H. Weng, Multi-loop node line states in ternary mgsrsi-type crystals, *npj Computational Materials* **5**, 10 (2019).
- [59] J. Lian, L. Yu, Q.-F. Liang, J. Zhou, R. Yu, and H. Weng, Multi-loop node line states in ternary mgsrsi-type crystals, *npj Computational Materials* **5**, 10 (2019).
- [60] A. Singh, M. Sebastian, Y. Chen, P.-Y. Chang, and A. Belyanin, Hyperbolic polaritons in topological nodal ring semimetals, *Phys. Rev. Lett.* **131**, 096902 (2023).

- [61] B. Roy, Interacting nodal-line semimetal: Proximity effect and spontaneous symmetry breaking, *Phys. Rev. B* **96**, 041113 (2017).
- [62] A. Alassaf, J. Kolta, and L. Oroszlány, Surface magnon spectra of nodal loop semimetals, *Phys. Rev. B* **109**, 035161 (2024).
- [63] R. M. Geilhufe, F. Guinea, and V. Jurićić, Hund nodal line semimetals: The case of a twisted magnetic phase in the double-exchange model, *Phys. Rev. B* **99**, 020404 (2019).
- [64] X. P. Yang, Y.-T. Yao, P. Zheng, S. Guan, H. Zhou, T. A. Cochran, C.-M. Lin, J.-X. Yin, X. Zhou, Z.-J. Cheng, Z. Li, T. Shi, M. S. Hossain, S. Chi, I. Belopolski, Y.-X. Jiang, M. Litskevich, G. Xu, Z. Tian, A. Bansil, Z. Yin, S. Jia, T.-R. Chang, and M. Z. Hasan, A topological hund nodal line antiferromagnet, *Nature Communications* **15**, 7052 (2024).
- [65] L. Muechler, Z. Guguchia, J.-C. Orain, J. Nuss, L. M. Schoop, R. Thomale, and F. O. von Rohr, Superconducting order parameter of the nodal-line semimetal naalsi, *APL Materials* **7**, 121103 (2019), https://pubs.aip.org/aip/apm/article-pdf/doi/10.1063/1.5124242/14562940/121103_1_online.pdf.
- [66] E. Cheng, W. Xia, X. Shi, Z. Yu, L. Wang, L. Yan, D. C. Peets, C. Zhu, H. Su, Y. Zhang, D. Dai, X. Wang, Z. Zou, N. Yu, X. Kou, W. Yang, W. Zhao, Y. Guo, and S. Li, Pressure-induced superconductivity and topological phase transitions in the topological nodal-line semimetal sras3, *npj Quantum Materials* **5**, 38 (2020).
- [67] L. Li, G.-X. Zhi, Q. Zhu, C. Wu, Z. Yang, J. Du, J. Yang, B. Chen, H. Wang, C. Cao, and M. Fang, Superconductivity in the nodal-line compound la₃pt₃bi₄, *Phys. Rev. Res.* **4**, L032004 (2022).
- [68] J. J. Gao, J. G. Si, X. Luo, J. Yan, Z. Z. Jiang, W. Wang, C. Q. Xu, X. F. Xu, P. Tong, W. H. Song, X. B. Zhu, W. J. Lu, and Y. P. Sun, Superconducting and topological properties in centrosymmetric pbtas2 single crystals, *The Journal of Physical Chemistry C* **124**, 6349 (2020).
- [69] A. Ikeda, S. R. Saha, D. Graf, P. Saraf, D. S. Sokratov, Y. Hu, H. Takahashi, S. Yamane, A. Jayaraj, J. Ślawińska, M. B. Nardelli, S. Yonezawa, Y. Maeno, and J. Paglione, Quasi-two-dimensional fermi surface of superconducting line-nodal metal casb₂, *Phys. Rev. B* **106**, 075151 (2022).
- [70] T. Ikenobe, T. Yamada, D. Hirai, H. Yamane, and Z. Hiroi, Superconductivity induced by doping holes in the nodal-line semimetal naalge, *Phys. Rev. Mater.* **7**, 104801 (2023).
- [71] W. Duan, J. Zhang, R. Kumar, H. Su, Y. Zhou, Z. Nie, Y. Chen, M. Smidman, C. Cao, Y. Song, and H. Yuan, Nodeless superconductivity in the topological nodal-line semimetal casb₂, *Phys. Rev. B* **106**, 214521 (2022).
- [72] H. Takahashi, S. Kitagawa, K. Ishida, M. Kawaguchi, A. Ikeda, S. Yonezawa, and Y. Maeno, S-wave superconductivity in the dirac line-nodal material casb₂, *Journal of the Physical Society of Japan* **90**, 073702 (2021), <https://doi.org/10.7566/JPSJ.90.073702>.
- [73] J. R. Badger, Y. Quan, M. C. Staab, S. Sumita, A. Rossi, K. P. Devlin, K. Neubauer, D. S. Shulman, J. C. Fettinger, P. Klavins, S. M. Kauzlarich, D. Aoki, I. M. Vishik, W. E. Pickett, and V. Taufour, Dirac lines and loop at the fermi level in the time-reversal symmetry breaking superconductor laniga2, *Communications Physics* **5**, 22 (2022).
- [74] T. Shang, S. K. Ghosh, M. Smidman, D. J. Gawryluk, C. Baines, A. Wang, W. Xie, Y. Chen, M. O. Ajeeesh, M. Nicklas, E. Pomjakushina, M. Medarde, M. Shi, J. F. Annett, H. Yuan, J. Quintanilla, and T. Shiroka, Spin-triplet superconductivity in weyl nodal-line semimetals, *npj Quantum Materials* **7**, 35 (2022).
- [75] M. Singh, P. Saha, V. Nagpal, and S. Patnaik, Superconductivity and weak anti-localization in nodal-line semimetal ntnts2, *Superconductor Science and Technology* **35**, 084003 (2022).
- [76] Y. Li, Z. Wu, J. Zhou, K. Bu, C. Xu, L. Qiao, M. Li, H. Bai, J. Ma, Q. Tao, C. Cao, Y. Yin, and Z.-A. Xu, Enhanced anisotropic superconductivity in the topological nodal-line semimetal in_xtas₂, *Phys. Rev. B* **102**, 224503 (2020).
- [77] T. Shang, J. Zhao, L.-H. Hu, J. Ma, D. J. Gawryluk, X. Zhu, H. Zhang, Z. Zhen, B. Yu, Y. Xu, Q. Zhan, E. Pomjakushina, M. Shi, and T. Shiroka, Unconventional superconductivity in topological kramers nodal-line semimetals, *Science Advances* **8**, eabq6589 (2022), <https://www.science.org/doi/pdf/10.1126/sciadv.abq6589>.
- [78] S.-Y. Guan, P.-J. Chen, M.-W. Chu, R. Sankar, F. Chou, H.-T. Jeng, C.-S. Chang, and T.-M. Chuang, Superconducting topological surface states in the noncentrosymmetric bulk superconductor pb-tase₂, *Science Advances* **2**, e1600894 (2016), <https://www.science.org/doi/pdf/10.1126/sciadv.1600894>.
- [79] S. Sur and R. Nandkishore, Instabilities of weyl loop semimetals, *New Journal of Physics* **18**, 115006 (2016).
- [80] R. Nandkishore, Weyl and dirac loop superconductors, *Phys. Rev. B* **93**, 020506 (2016).
- [81] Y. Wang and R. M. Nandkishore, Topological surface superconductivity in doped weyl loop materials, *Phys. Rev. B* **95**, 060506 (2017).
- [82] H. Shapourian, Y. Wang, and S. Ryu, Topological crystalline superconductivity and second-order topological superconductivity in nodal-loop materials, *Phys. Rev. B* **97**, 094508 (2018).
- [83] J. Ahn and B.-J. Yang, Higher-order topological superconductivity of spin-polarized fermions, *Phys. Rev. Res.* **2**, 012060 (2020).
- [84] A. Lau, T. Hyart, C. Autieri, A. Chen, and D. I. Pikulin, Designing three-dimensional flat bands in nodal-line semimetals, *Phys. Rev. X* **11**, 031017 (2021).
- [85] Z. Wu and Y. Wang, Nodal topological superconductivity in nodal-line semimetals, *Phys. Rev. B* **108**, 224503 (2023).
- [86] X. Wang and T. Zhou, Fragile topology in nodal-line semimetal superconductors, *New Journal of Physics* **24**, 083013 (2022).
- [87] R. Yano, S. Nagasaka, N. Matsubara, K. Saigusa, T. Tanda, S. Ito, A. Yamakage, Y. Okamoto, K. Takenaka, and S. Kashiyawa, Evidence of unconventional superconductivity on the surface of the nodal semimetal caag1-xpdxp, *Nature Communications* **14**, 6817 (2023).
- [88] P.-Y. Chang and P. Coleman, Parity-violating hybridization in heavy weyl semimetals, *Phys. Rev. B* **97**, 155134 (2018).
- [89] C. Cao, G.-X. Zhi, and J.-X. Zhu, From trivial kondo insulator ce₃pt₃bi₄ to topological nodal-line semimetal ce₃pd₃bi₄, *Phys. Rev. Lett.* **124**, 166403 (2020).
- [90] H.-T. Ma, X. Ming, X.-J. Zheng, J.-F. Wen, Y.-C. Wang, Y. Liu, and H. Li, Node-line dirac semimetal manipulated via kondo mechanism in nonsymmorphic cept₂si₂, *Phys. Rev. B* **107**, 075124 (2023).
- [91] L. Chen, C. Setty, H. Hu, M. G. Vergniory, S. E. Grefe, L. Fischer, X. Yan, G. Eguchi, A. Prokofiev, S. Paschen, J. Cano, and Q. Si, Topological semimetal driven by strong correlations and crystalline symmetry, *Nature Physics* **18**, 1341 (2022).
- [92] D. F. Liu, Y. F. Xu, H. Y. Hu, J. Y. Liu, T. P. Ying, Y. Y. Lv, Y. Jiang, C. Chen, Y. H. Yang, D. Pei, D. Prabhakaran, M. H. Gao, J. J. Wang, Q. H. Zhang, F. Q. Meng, B. Thiagarajan, C. Polley, M. Hashimoto, D. H. Lu, N. B. M. Schröter, V. N. Strocov, A. Louat, C. Cacho, D. Biswas, T. L. Lee, P. Steadman, P. Bencok, Y. B. Chen, L. Gu, T. Hesjeda,

- G. van der Laan, H. Hosono, L. X. Yang, Z. K. Liu, H. Q. Yuan, B. A. Bernevig, and Y. L. Chen, *Discovery of an anti-ferromagnetic topological nodal-line kondo semimetal* (2024), arXiv:2411.13898 [cond-mat.str-el].
- [93] Y.-X. Wang, X. Wang, and Y.-X. Li, Double local and double nonlocal andreev reflections in nodal-line semimetal-superconducting heterostructures, *Phys. Rev. B* **105**, 195402 (2022).
- [94] X. Wang, Y.-X. Wang, and Y.-X. Li, Quasi-periodic andreev reflection in topological nodal-line semimetals superconductor junctions, *Journal of Applied Physics* **132**, 134303 (2022).
- [95] I. Sodemann and L. Fu, Quantum nonlinear hall effect induced by berry curvature dipole in time-reversal invariant materials, *Phys. Rev. Lett.* **115**, 216806 (2015).
- [96] Q. Ma, S.-Y. Xu, H. Shen, D. MacNeill, V. Fatemi, T.-R. Chang, A. M. Mier Valdivia, S. Wu, Z. Du, C.-H. Hsu, S. Fang, Q. D. Gibson, K. Watanabe, T. Taniguchi, R. J. Cava, E. Kaxiras, H.-Z. Lu, H. Lin, L. Fu, N. Gedik, and P. Jarillo-Herrero, Observation of the nonlinear hall effect under time-reversal-symmetric conditions, *Nature* **565**, 337 (2019).
- [97] Z. Z. Du, H.-Z. Lu, and X. C. Xie, Nonlinear hall effects, *Nature Reviews Physics* **3**, 744 (2021).
- [98] S. Lai, H. Liu, Z. Zhang, J. Zhao, X. Feng, N. Wang, C. Tang, Y. Liu, K. S. Novoselov, S. A. Yang, and W.-b. Gao, Third-order nonlinear hall effect induced by the berry-connection polarizability tensor, *Nature Nanotechnology* **16**, 869 (2021).
- [99] N. Wang, D. Kaplan, Z. Zhang, T. Holder, N. Cao, A. Wang, X. Zhou, F. Zhou, Z. Jiang, C. Zhang, S. Ru, H. Cai, K. Watanabe, T. Taniguchi, B. Yan, and W. Gao, Quantum-metric-induced nonlinear transport in a topological antiferromagnet, *Nature* **621**, 487 (2023).
- [100] A. Gao, Y.-F. Liu, J.-X. Qiu, B. Ghosh, T. V. Trevisan, Y. Onishi, C. Hu, T. Qian, H.-J. Tien, S.-W. Chen, M. Huang, D. Bérubé, H. Li, C. Tzschaschel, T. Dinh, Z. Sun, S.-C. Ho, S.-W. Lien, B. Singh, K. Watanabe, T. Taniguchi, D. C. Bell, H. Lin, T.-R. Chang, C. R. Du, A. Bansil, L. Fu, N. Ni, P. P. Orth, Q. Ma, and S.-Y. Xu, Quantum metric nonlinear hall effect in a topological antiferromagnetic heterostructure, *Science* **381**, 181 (2023), <https://www.science.org/doi/pdf/10.1126/science.adf1506>.
- [101] K. Fujiwara and T. Morimoto, Interaction-induced nonlinear magnon transport in noncentrosymmetric magnets, *Phys. Rev. B* **111**, 014408 (2025).
- [102] Y. Ulrich, J. Mitscherling, L. Classen, and A. P. Schnyder, Quantum geometric origin of the intrinsic nonlinear hall effect (2025), arXiv:2506.17386 [cond-mat.mes-hall].
- [103] H. Wang, H. Liu, X. Feng, J. Cao, W. Wu, S. Lai, W. Gao, C. Xiao, and S. A. Yang, Intrinsic nonlinear spin hall effect and manipulation of perpendicular magnetization, *Phys. Rev. Lett.* **134**, 056301 (2025).
- [104] Y. Fang, J. Cano, and S. A. A. Ghorashi, Quantum geometry induced nonlinear transport in altermagnets, *Phys. Rev. Lett.* **133**, 106701 (2024).
- [105] Z. Liao, H. Zeng, E. Wang, and H. Huang, Berry curvature dipole and nonlinear hall effect in type-ii semi-dirac systems, *Small* **n/a**, 2409691, <https://onlinelibrary.wiley.com/doi/pdf/10.1002/smll.202409691>.
- [106] L. Li, C. Cui, R.-W. Zhang, Z.-M. Yu, and Y. Yao, Planar hall plateau in magnetic weyl semimetals, *Science Bulletin* **70**, 187 (2025).
- [107] D. Soranzio, E. Abreu, S. Houver, J. Dössiger, M. Savoini, F. Teppe, S. Krishtopenko, N. N. Mikhailov, S. A. Dvoretsky, and S. L. Johnson, Roles of band gap and kane electronic dispersion in the terahertz-frequency nonlinear optical response in hgcdte, *Phys. Rev. B* **110**, 094303 (2024).
- [108] K. Santhosh Kumar, M. Kinna, A. P., R. Dagar, S. Sharma, D. Swaraj, and D. S. Rana, Observation of anomalous nonequilibrium terahertz dynamics and a gapped topological phase in a semimetal CaIrO₃ thin film, *Phys. Rev. B* **109**, 115150 (2024).
- [109] J. Pettine, P. Padmanabhan, N. Sirica, R. P. Prasankumar, A. J. Taylor, and H.-T. Chen, Ultrafast terahertz emission from emerging symmetry-broken materials, *Light: Science & Applications* **12**, 133 (2023).
- [110] C. Rizza and A. Molle, Closing the thz gap with dirac semimetals, *Light: Science & Applications* **11**, 124 (2022).